Available online at www.sciencedirect.com
SCIENCE DIRECT
International Journal of Heat and Mass Transfer 49 (2006) 2113–2123
International Journal of HEAT and MASS TRANSFER
www.elsevier.com/locate/ijhmt

Direct numerical simulations of a planar jet laden with evaporating droplets

Thomas G. Almeida [1], Farhad A. Jaberi *

Department of Mechanical Engineering, Michigan State University, 2240 Engineering Building, East Lansing, MI 48824-1226, USA

Received 1 October 2005; received in revised form 23 November 2005
Available online 28 February 2006

Abstract

A direct numerical simulation (DNS) study is conducted on the various aspects of phase interactions in a planar turbulent gas-jet laden with non-evaporative and evaporative liquid droplets. A compressible computational model utilizing a finite difference scheme for the carrier gas and a Lagrangian solver for the droplet phase is used to conduct the numerical experiments. The effects of droplet time constant, mass-loading and mass/momentum/energy coupling between phases on droplet and gas-jet fields are investigated. Significant changes in velocity, temperature, density and turbulence production on account of the coupling between the liquid and gas phases are observed in non-isothermal jets with evaporating droplets. Most of these changes are attributed to the density stratification in the carrier gas that is caused by droplet momentum and heat transfer.

Keywords: Droplet-laden turbulent jet; Two-phase planar jet; Droplet evaporation; DNS

1. Introduction

Multiphase flows occur in a wide range of engineering applications. Ink jet printers, spray combustors, and fire prevention systems are obvious examples of physical situations for which the understanding of multiphase transport phenomena are very important. This work is focused on a specific class of multiphase flows, that of dilute turbulent free shear flows laden with a dispersed medium, either solid particles or evaporating droplets. It is an effort to understand the complex mass/momentum/energy interactions between gas and droplet phases in a two-phase planar jet.

The general features of the ''developed'' single-phase planar and round turbulent jets are well-established. Hinze [1], Pope [2], Bernard and Wallace [3] and others have discussed these flows in detail, noting the general characteristics of the self-preserving portion of the flow. The near-fields of shear layers and jets are mainly controlled by the Kelvin–Helmholtz instabilities and are strongly dependent on the inlet flow conditions and external forcing [4]. Stanley and Sarkar [5] studied two-dimensional shear layers and jets, noting the impact that external forcing has on the jet development. They found that, although the downstream growth was nearly unaffected by forcing at the inlet, the near-field was modified. They reported some interesting results related to the symmetry of 'weak' and 'strong' jet flows due to forcing. The simulations performed herein would be classified as strong using their convention.

The effects of temperature/density on the growth and stability of free jets were studied by Kennedy and Chen [6]. They found that ''cold jets'' tended to be significantly more stable than ''hot jets''. They also indicated a modification of the mean velocity profile, where the cold jets profile were 'narrower' and had a ''more gradual taper of velocity'' than their hot counterparts. These are explained by Colucci [7], who used the linear stability theory to show that with a lower density at the shear zone the jet is more

* Corresponding author. Tel.: +1 517 432 4678; fax: +1 517 353 1750.
E-mail address: jaberi@egr.msu.edu (F.A. Jaberi).
[1] Present address: General Dynamics-AIS, 1200 Joe Hall Drive, Ypsilanti, MI 48197, USA.

0017-9310/$ - see front matter © 2006 Elsevier Ltd. All rights reserved.
doi:10.1016/j.ijheatmasstransfer.2005.11.029

Nomenclature

B_M	mass transfer number
c_p	specific heat at constant pressure of fluid
c_L	specific heat of droplets
D	jet diameter
d_p	particle diameter
E	total energy
f_1	coefficient related to particle drag
f_2	coefficient related to particle heat and mass transfer
f_3	coefficient related to particle heat and mass transfer
h_α	specific enthalpy of species α
h^0_α	enthalpy of formation of species α
J^α_i	mass flux of species α in ith direction
K	thermal conductivity
Le_α	Lewis number of species α
L_v	latent heat of evaporation
m_p	mass of particle
Ma	Mach number
N_s	number of species
P	pressure
Pr	Prandtl number
q_i	heat transfer in ith direction
R^0	universal gas constant
R	molecular weight gas constant
Re	Reynolds number
r	radial position
r_0	jet radius
S_E	energy source term
S_{ui}	momentum source term in ith direction
S_ρ	mass source term
T	fluid temperature
T_p	particle temperature
T_m	mean gas temperature
T_{rms}	RMS of gas temperature
t	time
u_i	ith component of fluid velocity vector
u'_i	deviation from the mean velocity in ith direction
u_{cl}	centerline axial velocity
u_m	mean axial velocity
u_{rms}	root-mean-square of axial velocity
$\overline{u'v'}$	Reynolds stress
v_i	ith component of particle velocity vector
W_α	molecular weight of species α
X_i	ith component of Lagrangian particle position
x_i	ith component of Eulerian coordinate system
Y_α	mass fraction of species α
γ	ratio of specific heats of the fluid
η	coefficient related to particle energy
μ	fluid viscosity
ρ	fluid density
ρ_p	particle density
σ_{ij}	Newtonian fluid stress tensor
τ_p	particle time constant
$\dot{\omega}_\alpha$	scalar source/sink term

stable. He also found that the convective wave speed is biased towards the higher density stream. In summary, if the higher speed stream is of lower density than the lower speed stream, the Kelvin–Helmholtz instabilities will be attenuated. Add to that the effects of the particle drag, etc. and there are interesting modifications to the jet structure.

Despite challenges involved in measurements and computations of particle laden turbulent flows, there have been a significant number of published works on these flows [8–11]. For example, Crowe et al. [12] used numerical and experimental data to show that particle dispersion in free shear flows is controlled by large-scale vortical structures, and not so much by local diffusion due to particle concentration gradients. Armenio and Fiorotto [13] studied the importance of the different forces acting on particles. The intent was to determine which, if any, could be neglected in favor of computational efficiency. They found that the most important force is that due to particle drag.

Jaberi [14] conducted a study of fluid–particle thermal interactions in a particle-laden homogeneous turbulent flow. His findings indicate that the temperature of both the carrier gas and the dispersed phase are dependent upon various properties, such as the particle time constant and the mass-loading ratio. Mashayek [15–17], Miller and Bellan [18,19], and Miller [20] also used DNS to study the temperature field and the phase (heat, mass and momentum) interactions in droplet-laden homogeneous shear and temporal mixing layer turbulent flows. An important finding was that in homogeneous shear flows solid particles decrease the turbulent kinetic energy and increase the anisotropy of the flow, but the evaporation effect is usually in the direction of decreasing the anisotropy. Several different models for evaporation models were compared by Miller et al. [21]. They found that the non-equilibrium Langmuir–Knudsen model is the most accurate one. This model is used here.

As noted above, the main objective of this work is to study the droplet–carrier gas interactions in dilute, two-phase isothermal and non-isothermal planar jets with and without droplet evaporation. For reasons that are not discussed here, the calculations are based on an Eulerian–Lagrangian model and utilize a particle-source-in-cell (PSIC) methodology. This may not be considered a true DNS because the flow around each individual particle or droplet is not fully computed. However, a careful analysis of the results indicates that for the dilute systems and small (low Reynolds number) droplets studied here the point-

particle assumption is reasonably valid. The simulations discussed herein are 'pseudo-two-dimensional', for the longitudinal depth of the planar jet is small enough to keep the variations in the z-direction negligible.

2. Formulation and computational methodology

The Eulerian–Lagrangian mathematical model used here for the carrier gas phase and the dispersed phase (either solid particles or liquid droplets) is somewhat similar to that of Miller and Bellan [18]. The two-way mass, momentum, and energy coupling between the phases are modeled via the particle-source-in-cell method. The equations are derived under the assumptions of calorically perfect species (carrier gas and evaporate), no body forces (e.g., gravity) and the dispersed phase volume fraction much less than unity. The non-dimensional carrier gas (Eulerian) equations for total mass, momentum, energy and scalar (evaporate) mass fraction are

$$\frac{\partial \rho}{\partial t}+\frac{\partial \rho u_i}{\partial x_i}=S_\rho \tag{1}$$

$$\frac{\partial \rho u_i}{\partial t}+\frac{\partial \rho u_i u_j}{\partial x_j}=-\frac{\partial P}{\partial x_i}+\frac{1}{Re}\frac{\partial \sigma_{ij}}{\partial x_j}+S_{ui} \tag{2}$$

$$\frac{\partial \rho E}{\partial t}+\frac{\partial \rho E u_i}{\partial x_i}=-\frac{\partial P u_i}{\partial x_i}+\frac{1}{Re}\frac{\partial u_j \sigma_{ij}}{\partial x_i}-\frac{1}{(\gamma-1)Ma^2 RePr}\frac{\partial q_i}{\partial x_i}+S_{\mathrm{E}} \tag{3}$$

$$\frac{\partial \rho Y_\alpha}{\partial t}+\frac{\partial \rho Y_\alpha u_i}{\partial x_i}=-\frac{1}{RePrLe_\alpha}\frac{\partial J_i^\alpha}{\partial x_i}+\dot{\omega}_\alpha \tag{4}$$

The pressure, gas constant, Newtonian shear stress, heat flux, mass flux, total energy and enthalpy in Eqs. (1)–(4) are obtained from the following equations:

$$P=\frac{1}{\gamma Ma^2}\rho RT \tag{5}$$

$$R=R_u\sum_\alpha \frac{Y_\alpha}{W_\alpha} \tag{6}$$

$$\sigma_{ij}=\mu\left(\frac{\partial u_i}{\partial x_j}+\frac{\partial u_j}{\partial x_i}-\frac{2}{3}\delta_{ij}\frac{\partial u_k}{\partial x_k}\right) \tag{7}$$

$$q_i=-\mu\left(c_p\frac{\partial T}{\partial x_i}+\sum_\alpha \frac{h_\alpha}{Le_\alpha}\frac{\partial Y_\alpha}{\partial x_i}\right) \tag{8}$$

$$E=\frac{1}{(\gamma-1)Ma^2}\sum_\alpha h_\alpha Y_\alpha-\frac{P}{\rho}+\frac{u_i u_i}{2} \tag{9}$$

$$h_\alpha=h_\alpha^0+c_{p\alpha}T \tag{10}$$

It should be noted that for a perfect non-reacting binary mixture (of the carrier gas and the evaporate) we only need one scalar equation with $\alpha=1,\ \dot{\omega}=S_\rho$. The Lagrangian equations for the droplets or particles are defined by

$$\frac{\mathrm{d}X_i}{\mathrm{d}t}=v_i \tag{11}$$

$$\frac{\mathrm{d}v_i}{\mathrm{d}t}=\frac{f_1}{\tau_\mathrm{p}}(u_i-v_i)=\frac{F_i}{m_\mathrm{p}} \tag{12}$$

$$\frac{\mathrm{d}T_\mathrm{p}}{\mathrm{d}t}=\frac{\eta f_2}{\tau_\mathrm{p}}(T-T_\mathrm{p})+\frac{L_\mathrm{v}}{m_\mathrm{p}c_\mathrm{L}}\frac{\mathrm{d}m_\mathrm{p}}{\mathrm{d}t}=\frac{Q_\mathrm{conv}+L_\mathrm{v}\dot{m}_\mathrm{p}}{m_\mathrm{p}c_\mathrm{L}} \tag{13}$$

$$\frac{\mathrm{d}m_\mathrm{p}}{\mathrm{d}t}=-\frac{m_\mathrm{p}f_3}{\tau_\mathrm{p}}\ln(1+B_\mathrm{M})=\dot{m}_\mathrm{p} \tag{14}$$

The subscript p indicates the droplet property, and the fluid properties are interpolated to the droplet position. The value of f_1 is empirically evaluated for the Stoke's drag, based on the droplet slip and blowing Reynolds numbers, Re_sl and Re_b. Similarly, f_2 and f_3 are functions of the droplet properties, both involving heat and mass transfer properties, such as the Nusselt number (Nu), Prandtl number (Pr), Sherwood number (Sh) and Schmidt number (Sc). L_v, c_L and B_M are the droplet heat of vaporization, heat capacity and mass transfer number, respectively, and the particle/droplet time constant is defined as

$$\tau_\mathrm{p}=\frac{Re\rho_\mathrm{p}d_\mathrm{p}^2}{18\mu} \tag{15}$$

Evaporation is taken into account via the Langmuir–Knudsen evaporation model, which takes into account both equilibrium and non-equilibrium effects. Finally, the two-way coupling effects are taken under consideration through the use of the source terms which, for mass, momentum and energy, are defined as

$$S_\rho=-\frac{1}{\delta V}\sum_{np}\dot{m}_\mathrm{p} \tag{16}$$

$$S_{ui}=-\frac{1}{\delta V}\sum_{np}(F_i+\dot{m}_\mathrm{p}v_i) \tag{17}$$

$$S_\mathrm{E}=-\frac{1}{\delta V}\sum_{np}\left(\frac{Q_\mathrm{conv}}{(\gamma-1)Ma^2}+v_iF_i+\dot{m}_\mathrm{p}\left(\frac{h_{v,s}}{(\gamma-1)Ma^2}+\frac{v_iv_i}{2}\right)\right) \tag{18}$$

These source terms are evaluated by summation of particle values over a finite Eulerian volume, δV.

The carrier gas Eulerian equations are solved with a fourth-order compact finite differencing scheme. The dispersed phase equations are calculated with a second-order explicit method. The carrier gas properties are interpolated to the droplet position via first-order linear and fourth-order Lagrange polynomial. The accuracy of the linear interpolation was determined to be sufficient to resolve the interaction between phases here (see Fig. 1), and thus was used in the majority of simulations. The jet inlet mean velocity profile chosen is hyperbolic tangent and the jet is subjected to random-phase harmonic forcing at the shear layer in the transverse (y) direction. The forcing energy peak is set at 5% for each of five frequencies, the harmonic, one super-harmonic and three sub-harmonics. Each harmonic has a randomly generated time variable phase. The phase angles applied to the top shear region are different than those applied to the bottom region. The inlet and outlet boundary conditions (BCs) are based on non-reflecting BC of Poinsot and Lele [22] and that of Rudy and Strikewerda [23]. The y-direction BCs are chosen to be

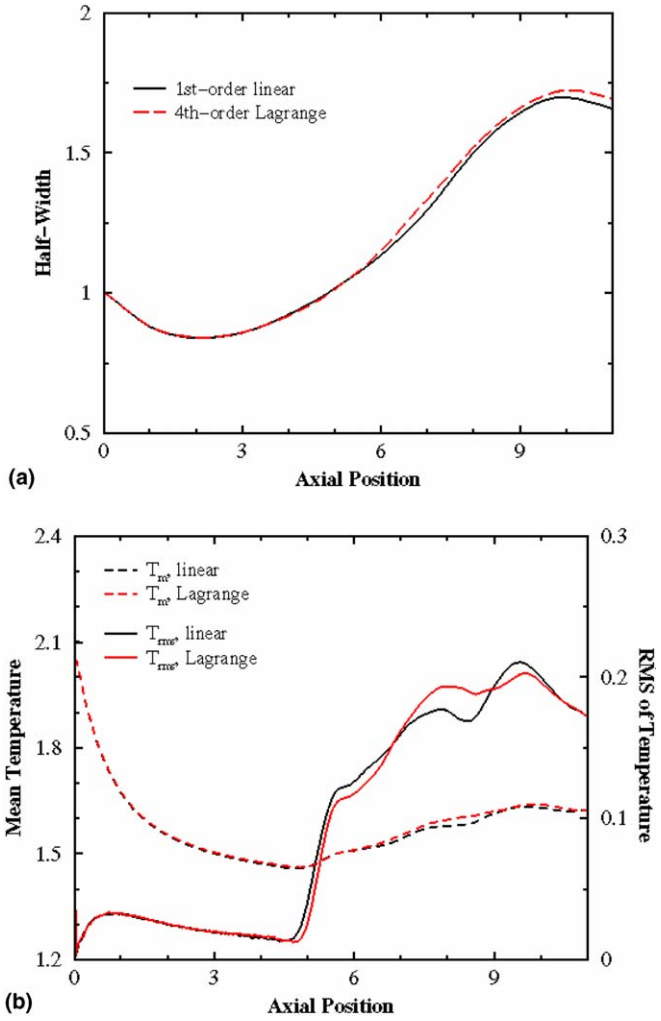

Fig. 1. (a) Half-width of jet, (b) mean and root-mean-square (RMS) of temperature for various interpolation schemes.

zero-derivative free-stream, and the z-direction BCs were periodic.

The statistical properties are obtained by time-averaging over at least three pass-over times, $t_{\text{pass}} = \frac{x_{\max}}{(u_{\text{jet}}+u_{\text{co}})/2}$. Convergence is confirmed via comparison between the mean and RMS properties at two different times, noting less than 1% difference. The jet is given one and a half pass-over times to develop initially before the averaging is started.

3. Results and discussion

Some of the physical parameters for the numerical simulations are presented in Table 1. These simulations are chosen to emulate a planar jet of air laden with droplets of decane. The parameters can easily be modified to more closely match other physical configurations. Two different sets of simulations are considered: (i) simulations without droplet evaporation and (ii) simulations with droplet evaporation.

To verify the accuracy of the numerical schemes used in this study, various tests were devised and implemented. For example, two different interpolation schemes were implemented for this work: first-order linear and fourth-order Lagrange polynomial. The results for the two cases were compared, and the accuracy of the linear interpolation was determined to be sufficient. The case used for comparison was the most complicated physically, including evaporative effects at high temperatures. Fig. 1 shows the jet half-width growth rate and the temperature profiles of the two interpolation schemes. While there are some differences to be noted, the two are within an acceptable margin of accuracy.

Table 1
Some physical parameters of the carrier fluid and the droplets

Carrier fluid	Air
Dispersed phase	Decane droplets
Jet Reynolds number	3165
Jet Mach number	0.291
Prandtl number	0.75

3.1. Non-evaporating droplets

Both one-way and two-way coupling cases are considered in this section. In the one-way coupling cases, the effects of carrier gas on the droplets are studied. The droplets do not have any effect on the carrier gas, and are spherical and non-evaporating. We therefore refer to these droplets as particles in the discussion that follows. Fig. 2 shows the effects of particle injection location on the particle number density or particle dispersion for $\tau_p = 1$. It is observed that the downstream behavior of the particles is not very much dependent on the shape of particle distribution or injection at jet inlet. This is only valid in one-way coupling cases, as the particle concentration in the shear layer affects the growth of instabilities and the results are sensitive to inlet/initial particle distribution in two-way coupling cases.

Fig. 2 also indicates that the particles are preferentially concentrated in "thin layers" at downstream locations. The effects of particle inertia on particle dispersion are not shown in Fig. 2. However, for both small and large particles, the particle dispersion is generally less than that for intermediate size particles with $\tau_p = 1$. This is demonstrated in Fig. 3(a), where it is shown that the number of particles integrated over the cross-stream (y) direction is relatively constant for large or high inertia particles ($\tau_p = 100$), erratic for intermediate size particles ($\tau_p = 1.0$), and approximately harmonic farther downstream for small particles ($\tau_p = 0.01$). As expected, the small particles behave like fluid particles with a nearly harmonic behavior due to harmonic forcing of the jet and the large ones do not respond to changes in the fluid. Fig. 3(b) shows the transverse variation of particle number density as it relates to particle size. The striking characteristic of the flow observed in this figure is what we call "local particle dispersion". Both the small and the large particles

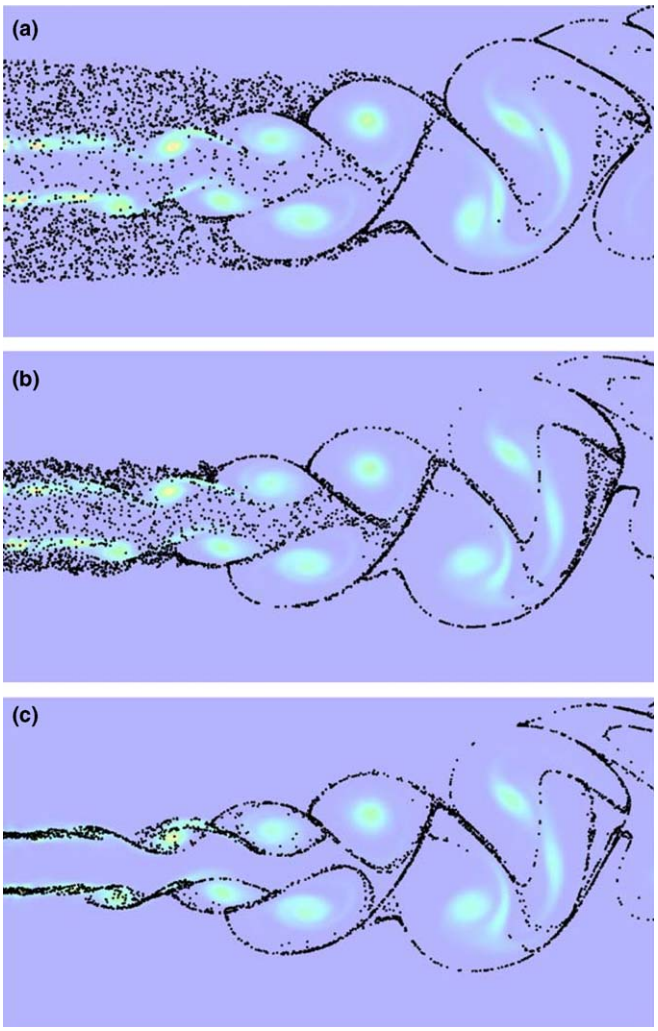

Fig. 2. Particle dispersion for various inlet particle distribution or injection location. (a) Uniform injection over $4h$ (h is the jet width), (b) uniform injection over $2h$, and (c) injection at shear layer over $2\Delta y$ (Δy is the grid thickness in the cross-stream direction). The particle time constant, τ_p is 1.0 in all cases.

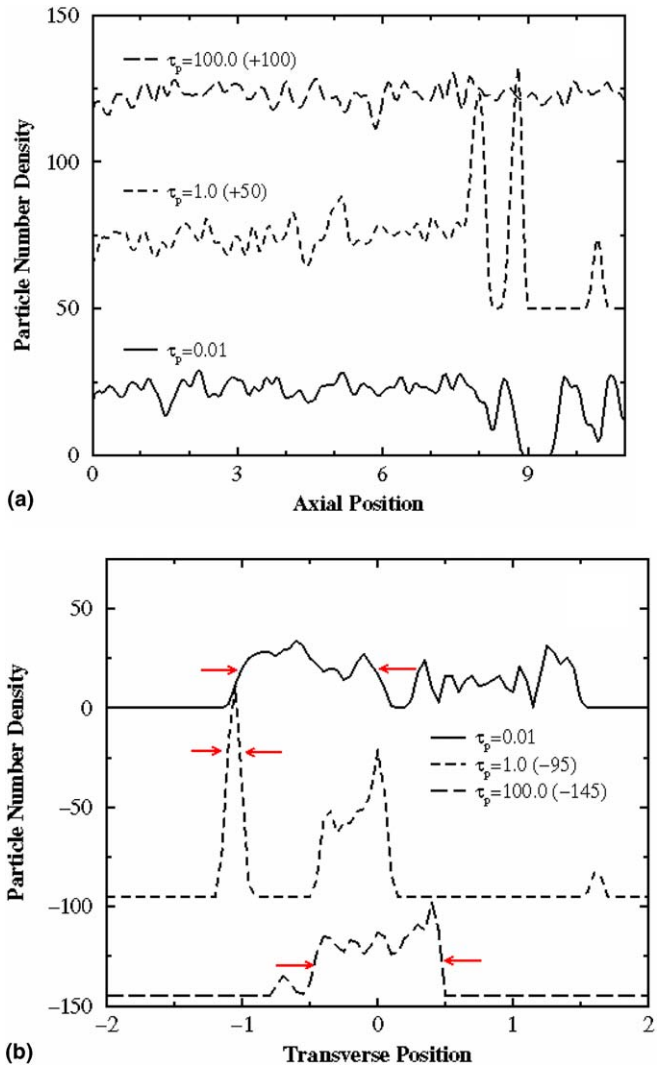

Fig. 3. Particle inertia effects on particle number density. (a) Axial profiles of integrated particle number density (the plots for the larger particles are shifted upward for clarity), (b) particle number density transverse profiles at $x/h = 8$ (the plots for $\tau_p = 1.0$ and $\tau_p = 100.0$ cases are shifted downward for clarity).

have regions of high particle dispersion, while the line corresponding to the intermediate size particles ($\tau_p = 1.0$) clearly shows minimal local particle dispersion in the narrow width and high peaks of the high particle density regions which is consistent with the results in Fig. 2. For the other τ_p values, the high particle density regions are broader and, on average, less dense. This has important implications when evaporative and/or reactive particles/droplets are considered.

For the two-way coupling cases considered in this section, the energy and momentum source terms affect the carrier gas; however the droplets are still non-evaporating. This allows for realistic physical simulations with two-way coupling effects present, but removing the complexities due to evaporation and mass coupling. The effects of particle size, mass-loading ratio and carrier gas temperature are investigated in details by considering several different cases (Table 2). Case 7 was conducted to examine the modifications due to the temperature-dependency of density and viscosity, and to separate from those the effects of the particles as 'temperature sinks' on the carrier gas field. The results of Cases 1, 2 and 3 aid in the understanding of

Table 2
Carrier fluid and droplet (particle) parameters for non-evaporating and two-way coupling cases

Case	τ_p	ϕ_m	T
1	0.1	0.2184	293
2	1.0	0.2184	293
3	10.0	0.2184	293
4	1.0	0.2908	293
5	1.0	0.3637	293
6	1.0	0.4365	293
7	1.0	0.4472	600 ($dT_p/dt = 0$)
8	1.0	0.4472	600

the effects of particle size on various turbulent properties. Cases 2, 4, 5 and 6 were designed to study the effects of particle mass-loading and Cases 2, 7 and 8 help in understanding the effects of the carrier gas temperature distributions on the particle temperature and jet development.

As expected, Fig. 4 shows that the particles' influence on the carrier gas increases with an increase in mass-loading ratio. Clearly, there is a significant decrease in the slope of the linear growth region with an increase in mass-loading ratio. Using the mass-loading as the independent variable (X) and the slope of the half-width in the self-similar region as the dependent variable (Y), a linear regression analysis yields $Y = -0.105X + 0.128$, $r = -0.989$; this implies the linear effects of mass-loading on jet growth rate.

Fig. 5 shows the jet half-width growth rate for different particle sizes. The results confirm the existence of "ghost particles", which were hypothesized by Ferrante and Elghobashi [24]. The larger particles damp the Kelvin–Helmholtz instabilities which, in turn, decrease the growth rate of the jet; yet the addition of tiny particles slightly increases the jet growth rate. Therefore, it seems entirely probable that there is a particular particle size that will have a minimal effect on the jet. A poignant finding is that the particle with $\tau_p = 1.0$ have the largest damping effect on the carrier gas. Physically this could be explained as particles that have a particle response time that is on the order of the time scale of the carrier gas kinetic energy will tend to dissipate the energy in a way similar to added viscous effects. The non-linearity of the correlations for particle drag make it difficult to analyze (or verify) the effect of particle inertia on transitional and turbulent jet directly from a theory.

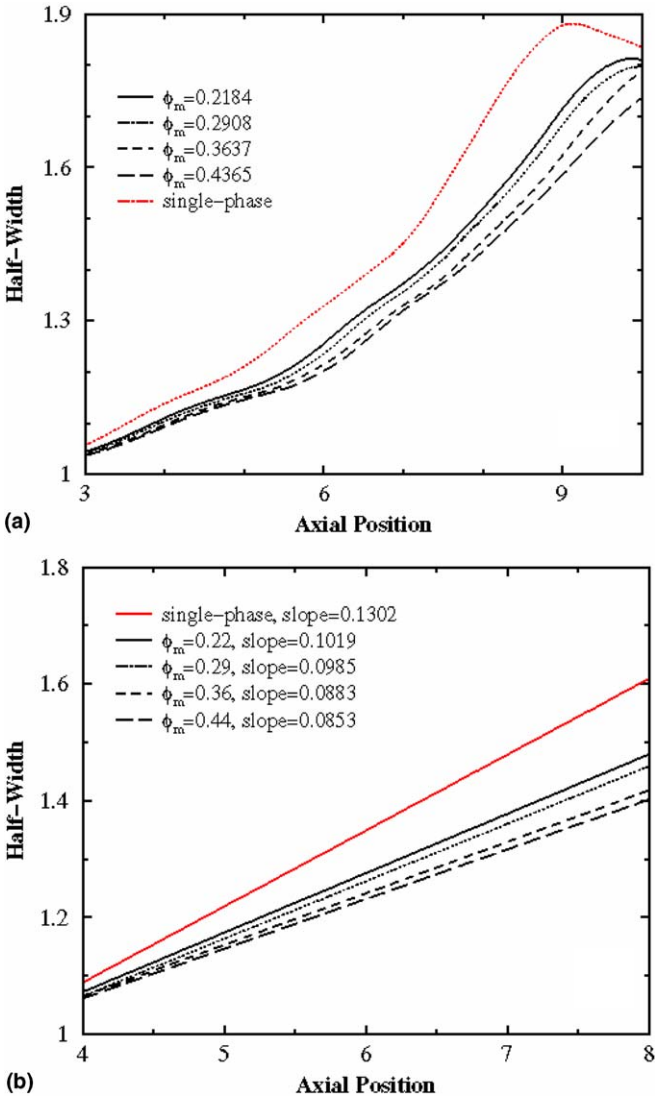

Fig. 4. Effect of mass-loading on jet growth rate. (a) DNS results and (b) fitted lines in the self-preserving region. $\tau_p = 1.0$ in all cases.

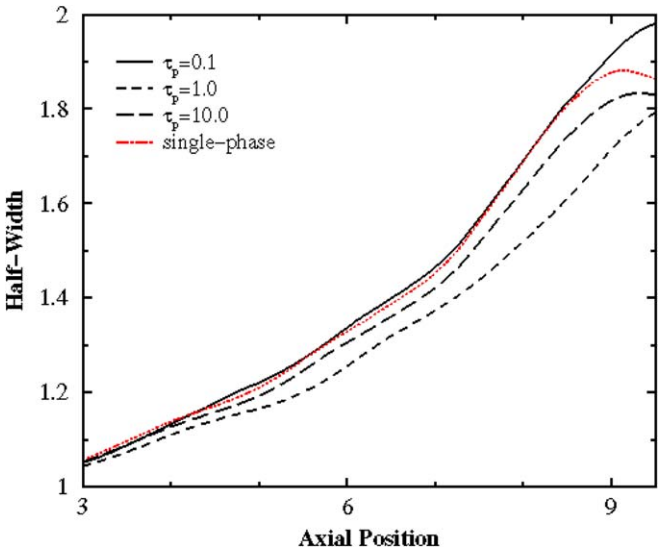

Fig. 5. Effects of particle time constant on jet growth rate. The slopes of the fitted lines in the "self-preserving" region ($4 < x/h < 8$) are 0.1302 for single-phase jet and 0.1316, 0.1019, 0.1203 for two-phase jets with $\tau_p = 0.1$, 1.0, 10.0, respectively.

The centerline mean axial velocity of a single-phase planar turbulent free jet decays as $x^{-1/2}$ in the self-similar region [2]. This decay rate is expected to be decreased by the addition of large particles. Fig. 6(a) shows the centerline axial velocity profiles in our forced jet simulations. Note the decrease in jet mean velocity decay rate as the mass-loading ratio is increased. The root-mean-square (RMS) of axial velocity exhibits trends similar to mean axial velocity at the center line: lesser growth rate for larger mass-loading. The RMS value reaches a higher peak earlier in the flow with lower mass-loading. Then it decays faster than that observed for higher mass-loading ratios. There is a 'cross-over' point around $x/h = 9$. Another important variable to consider when investigating planar jets is the Reynolds stress, $\overline{u'v'}$, that appears in the production term of the turbulent kinetic energy equation. For convenience, here we consider the space averaged values of the Reynolds stress. For example, Fig. 6(b) shows the variation of $\frac{1}{2 \cdot y_{max}} \int \overline{u'v'}\, dy$ versus x for different mass-loading ratio. Evidently, the integrated values of the Reynolds stress in the transverse direction in two-phase jet is negative with a

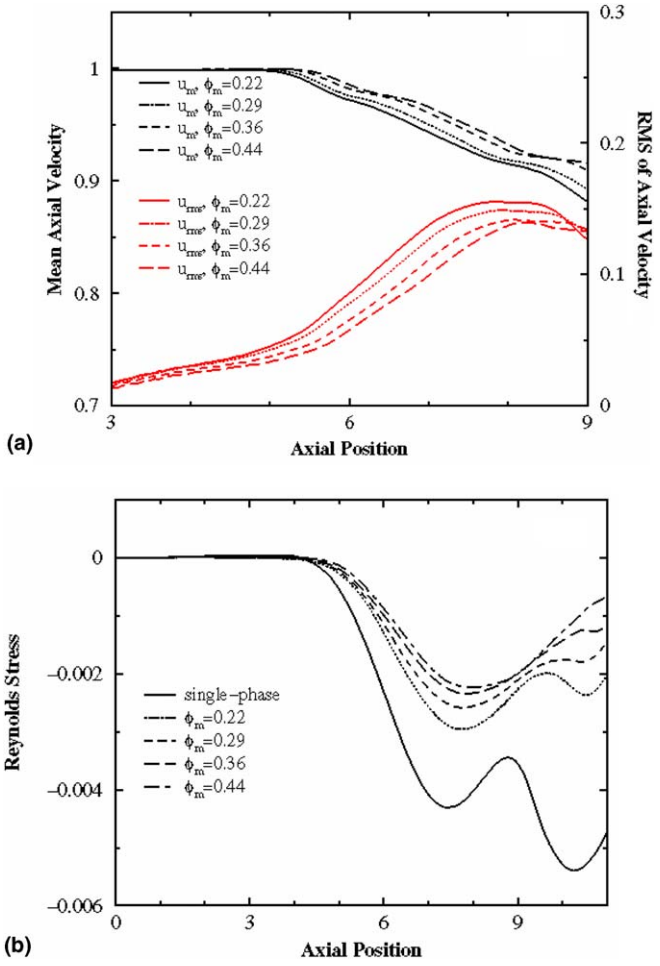

Fig. 6. (a) Centerline mean axial velocity, u_m profiles as a function of mass-loading and (b) axial variation of integrated Reynolds stress profiles versus mass-loading. $\tau_p = 1.0$ in all cases.

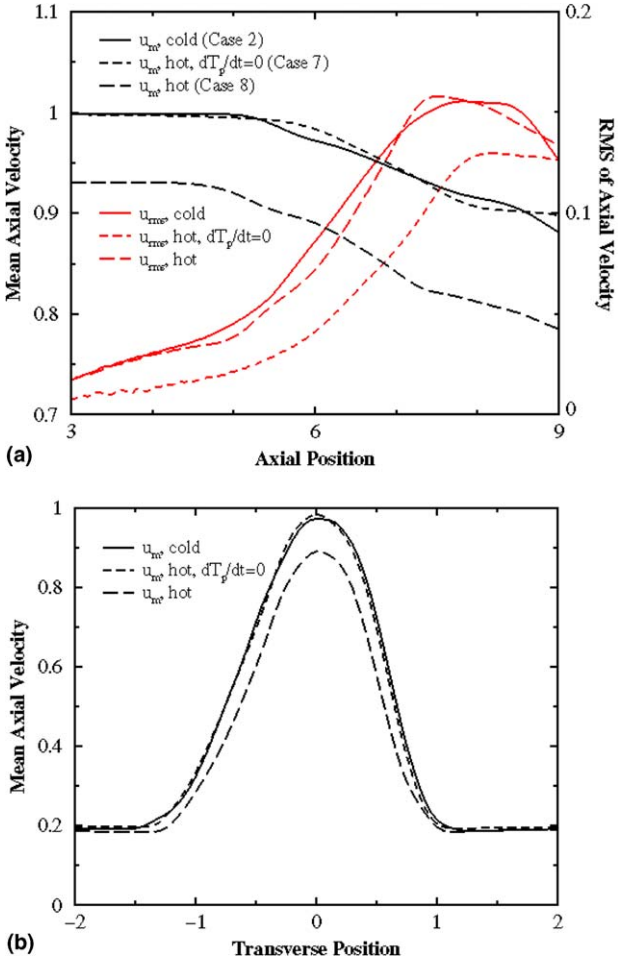

Fig. 7. Particle effects on jet for two-way coupling cases. (a) Mean axial velocity, u_m and RMS of axial velocity, u_{rms} at jet centerline and (b) transverse variation of mean axial velocity at $x/h = 6$.

magnitude considerably less than that in single-phase one. This is consistent with the results in Fig. 5. When particles with moderate inertia ($\tau_p = 1.0$) are added to the flow, the overall growth of the Reynolds stress is severely hampered, resulting in an increase in the stability of the jet.

The axial variation of the centerline mean and RMS values of the axial velocity and the transverse variation of the mean axial velocity for Cases 2, 7 and 8 are shown in Fig. 7. The non-evaporating non-isothermal two-way coupling Cases 7 and 8 involve interesting aspects of the particles' thermal inertia and the heat transfer between phases in a planar jet. To exclude the density effects on jet growth, a non-physical case (Case 7) is considered in which the two-way thermal interactions between particles and carrier gas is not allowed. The realistic physical case (Case 8) involves much more complicated particle–gas interactions. For one, the particles act as temperature sinks, decreasing the carrier gas temperature in the core of the flow. This causes a density stratification wherein the high speed flow is cooler (and thus denser) than the low speed flow. This acts to stabilize the jet, decreasing the growth rate [7]. It also causes the entrainment velocity to change (Fig. 7). However, the thermal interactions between phases seem to have a rather complicated effect on the jet velocity field. When the particles are not allowed to have two-way thermal interactions with the gas, the mean axial jet velocity is nearly unchanged, while the RMS of axial velocity is significantly damped due to momentum coupling, especially in the region where the particles are concentrated. When the particles have two-way momentum and heat interactions with the carrier gas, the centerline mean axial velocity is attenuated, while the RMS of axial velocity is nearly unchanged! This implies that the particle thermal inertia has two conflicting effects on the velocity field. On one hand it enhances the turbulent velocity fluctuations in the jet, on the other hand it tends to damp the instabilities and the overall jet growth rate through the induced fluid density stratification.

Fig. 8 illustrates how the thermal coupling and changes in the carrier gas temperature affect the particle velocity field. The results in this figure show the instantaneous "Eulerian" axial particle velocity field as obtained by volume averaging of the individual particle velocities. Evidently, the particle axial velocity near the jet centerline is

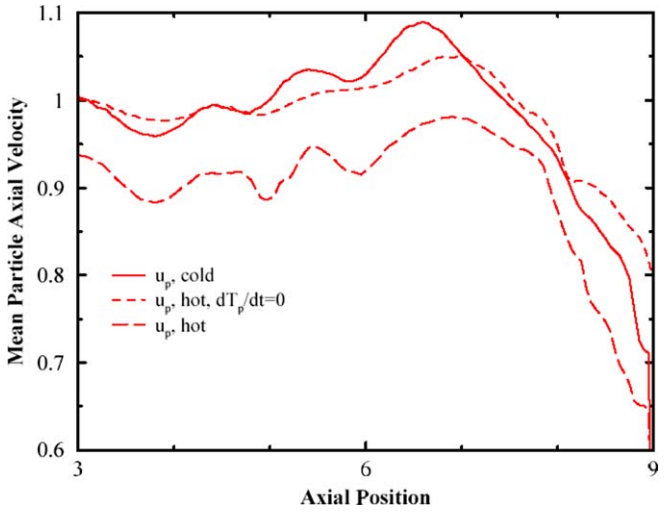

Fig. 8. Axial variation of the instantaneous particle axial velocity, u_p at jet centerline for various two-way coupling cases.

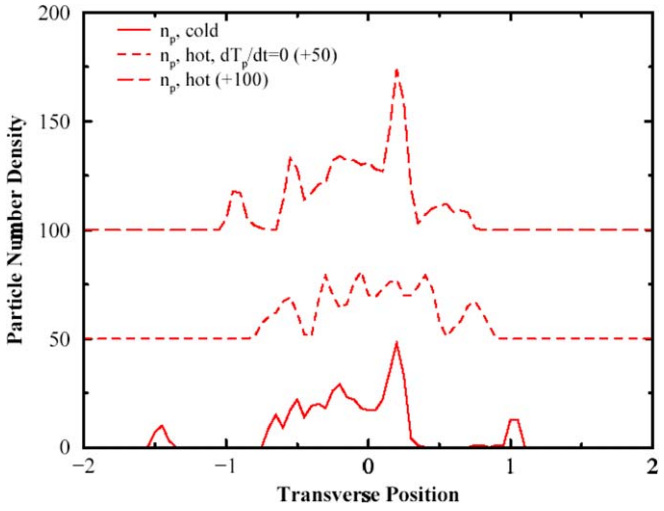

Fig. 9. Transverse variation of the particle number density, n_p at $x/h = 6$ for various two-way coupling cases.

considerably lower in the high-temperature case as compared to that in the low-temperature case. In the non-physical Case 7 with $dT_p/dt = 0$, the density stratification causes a relatively smooth particle velocity profile. This supports the notion that this form of temperature (or density) variation in the particle field reduces turbulent fluctuations of the carrier gas.

The effects of thermal coupling and variable temperature/density fields on particle distribution and preferential concentration is shown in Fig. 9. The results in this figure indicate that the particles in the high-temperature case (Case 8) tend to stay closer to the centerline of the jet, and thus accumulate more readily than those in the low-temperature case (Case 2).

3.2. Evaporating droplets

There are several important effects that droplet evaporation has on the gas and droplet fields in a planar jet. These

Table 3
Description of cases relevant to the investigation of droplet evaporation effects on the jet

Case number	Description
1	Single-phase/one-way coupling without evaporation
2	One-way coupling with density stratification without evaporation
3	Two-way coupling, with $dT_p/dt = 0$ without evaporation
4	Two-way coupling without evaporation
5	Two-way coupling with evaporation

are best understood when the evaporative effects are separated from those caused by the momentum and heat interactions between phases. Table 3 describes the cases that are relevant to our discussion on jets laden with evaporating droplets, and Fig. 10 shows the growth rate of the jet half-width and the centerline velocity for these cases. These cases are selected in support of our systematic investigation of the various competing mechanisms in a droplet-laden planar jet flow. Cases 1, 2 and 5 provide a progression of

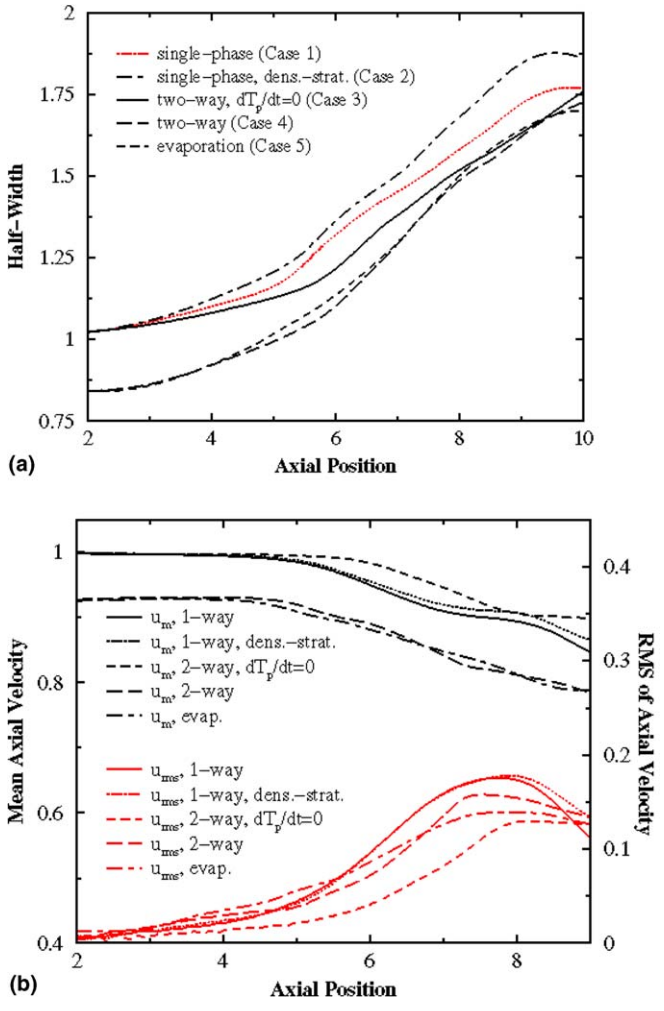

Fig. 10. Jet statistics for different cases with and without droplet evaporation. (a) Jet half-width, (b) mean axial velocity, u_m and RMS of mean axial velocity, u_{rms} at jet centerline.

comparisons between a single-phase hot jet in a hot co-flow, a cooler jet in a hot co-flow, and a fully coupled evaporative case wherein the temperature of the jet is similar to that in the density stratified (single-phase) case. Comparing results for Cases 1 and 3 show the effects of momentum coupling between solid particles and the carrier fluid. Case 4 emphasizes the effect of the thermal interactions between phases, and Case 5 is the penultimate case, adding the effects of evaporation to Case 4.

Fig. 10(a) indicates that in the absence of heat or mass interactions between phases the addition of droplets does not significantly change the jet growth rate at $5 < x/h < 9$. However, when the temperature effects of the particles on the carrier gas are included, there is a significant change in the jet growth rate. The modification to the jet growth as caused by non-uniform inlet temperature/density distribution in single-phase flow simulation is slightly less than that due to particles in the two-phase two-way coupled case. Also, when the effects of evaporation are included, the jet growth rate is less as compared to that without evaporation. The density stratification seems to contribute significantly, but not exclusively to the modification of the jet growth rate. What is interesting in Fig. 10(b) is the changes that particles make on the RMS of axial gas velocity, as the difference between the (two-way couplings) cases with and without evaporation is more evident in the velocity fluctuations. The tendency of the RMS of axial velocity to decay after reaching its peak is lower in the evaporative case. It seems that the added mass due to evaporation decreases the peak value, but sustains the turbulence levels further beyond that peak.

The Reynolds stress profiles for different one-way and two-way coupling cases are shown in Fig. 11. These are obtained by averaging over the direction normal to the direction of interest. Note the considerable modifications in the Reynolds stress profiles which are due to droplet evaporation. Specifically, there is a considerable overall decrease in the Reynolds stress for the two-way coupled case without evaporation. The case with evaporation showed an increase in Reynolds stress over the two-way coupled case without evaporation except between $x/h \approx 7$ and 9. A decrease in the Reynolds stress decreases the turbulent production, which can be generally associated with a decrease in the velocity fluctuations, effectively increasing the stability of the jet. Hence, a decrease in the growth rate of the jet is to be expected. Indeed our results (not shown here) indicate an increase in the peak of the production of turbulent kinetic energy from the non-evaporating to the evaporating case near $x/h \approx 9$. There is also an increase in the production of turbulent kinetic energy in the evaporation case over the one-way case with density stratification. The density stratification increases the turbulent production initially, followed by a steady decline towards the values predicted by the one-way coupled simulation with uniform density. The larger variation in the production of turbulent production rate in the near-field region as compared to the relatively uniform values of the Reynolds stress is a good indication of the modification to the mean velocity of the gas velocity fluctuations.

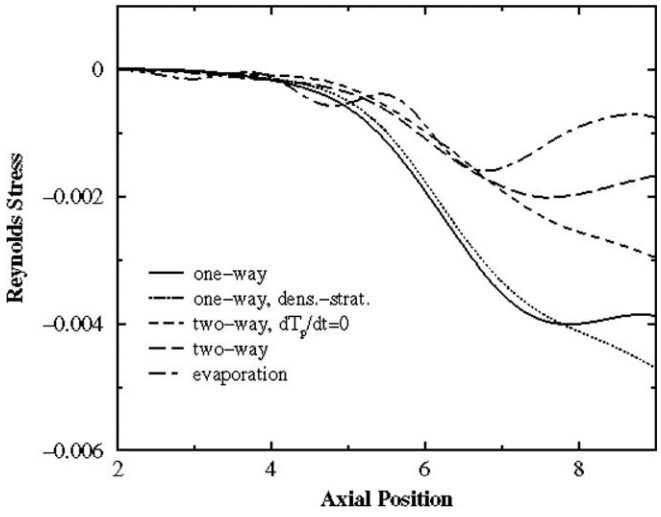

Fig. 11. Axial variation of Reynolds stress for different cases with and without evaporation.

Further examination of the axial velocity of the particles in Cases 4 and 5 indicate that the jet with evaporative droplets behaves remarkably similar to the one with non-evaporating droplets in the near-field region. Farther downstream, the droplets have evaporated enough so that they behave more like smaller particles as opposed to larger ones. Also, the properties of the carrier gas have been altered enough to create an environment similar to the density stratified case.

The effects of evaporation are generally attributed to several competing physical mechanisms. For example, the "cold" particles in the hot environment will act as temperature sinks even without evaporation, but the droplet evaporation will decrease the temperature even more, a natural consequence of change in latent energy. The axial variations of the gas temperature for evaporating and non-evaporating cases in Fig. 12(a) clearly show a nearly constant reduction in temperature along the jet by droplets. The value of this reduction is about 0.2 non-dimensional temperature units, or approximately 55 K, consistent with the parameters used in these simulations. The one-way density stratified case seems to agree more favorably with the two-way coupled case that has no evaporation than the one with evaporation, suggesting that the momentum and heat of evaporate vapor/gas in the evaporative case uniquely modifies the jet temperature and velocity fields. In addition to its effects on temperature, the evaporate vapor will also contribute mass, naturally adding to the density of the carrier gas. These combined effects may explain the observed differences between the cases with and without evaporation. The variation in the density and mass fraction of vapor as caused by heat/momentum transfer and evaporate added mass effects are shown in Fig. 12(b). It is to be noted that the non-dimensionalization of the variables allows us to directly add or subtract the

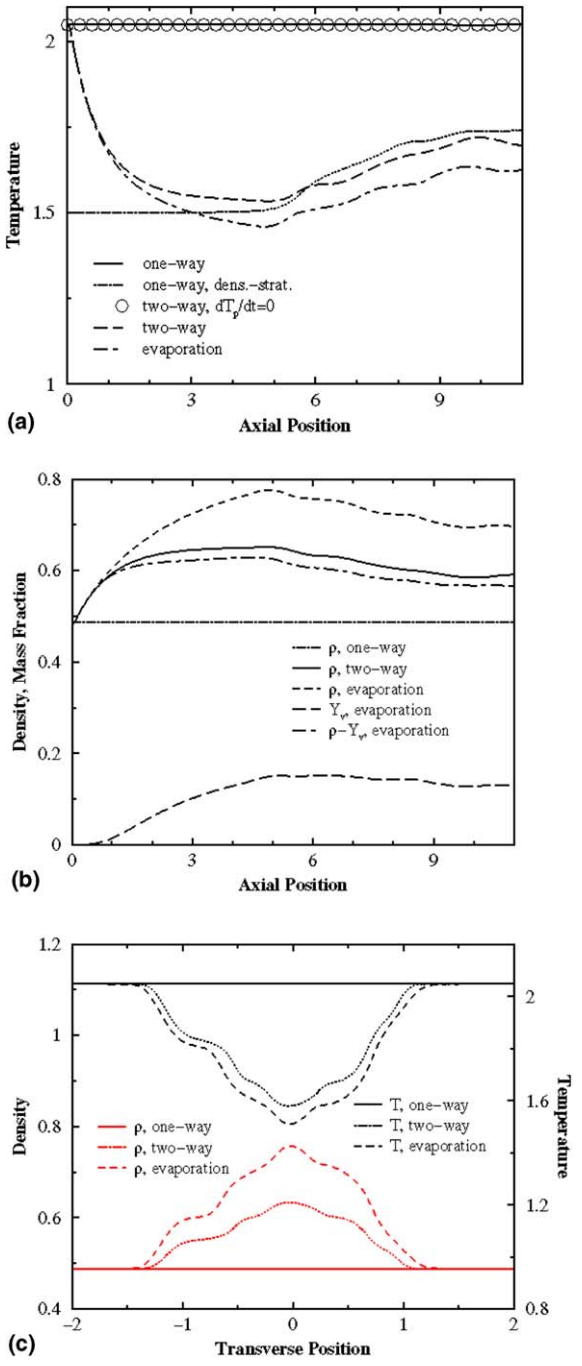

Fig. 12. (a) Temperature variation in the axial direction, (b) density and mass fraction of vapor variation in the axial direction, (c) temperature and density variation across the jet at $x/D = 6$ for various one- and two-way coupling cases.

density and the mass fractions. The difference in density between the two-way coupled cases with and without evaporation is nearly mimicked by the mass fraction of the evaporate gas. There is, however, a small difference between these two which is due to the actual heat of vaporization of the droplets modifying the temperature and density fields. The transverse variation of temperature and density are shown in Fig. 12(c).

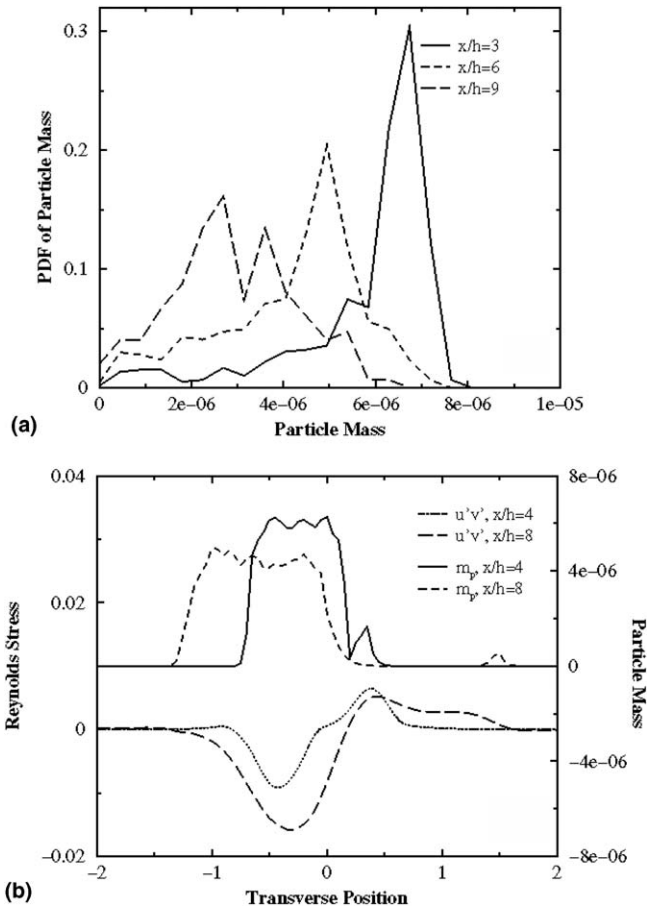

Fig. 13. (a) Development of the probability distribution function of particle mass. (b) Eulerian averaged particle mass and Reynolds stress profiles at various downstream locations.

As noted previously, different sizes of droplets or particles have different effects on the carrier gas (and the carrier gas affects them differently as well). Clearly, if droplets evaporate at different rates, there will then be a size distribution which could cause interesting modifications to the statistical properties of the turbulent jet. The development of the probability distribution function (PDF) of particle mass along the jet for $\tau_p = 1.0$ case is shown in Fig. 13(a). The PDF of particle mass at the inlet is a delta function, as the injected particles have uniform size. As the flow develops and droplets begin to evaporate, the PDF changes towards a more Gaussian shape, indicating that there are droplets which are not evaporating very much or are vaporizing very rapidly. The results do not allow for the discernment of local vaporization rates, as it represent the PDFs of all of the particles at a particular axial location (collected over cross-stream or y direction). Fig. 13(b) shows a comparison of the local average particle mass and the Reynolds stress. The transverse profiles show that, at locations where the droplets have significantly evaporated (i.e. droplets are small), there is an increase in the Reynolds stress. This seems to correlate well with the notion that smaller particles enhance the velocity fluctuations, while larger ones attenuate these fluctuations.

4. Conclusions

Direct numerical simulations (DNSs) of droplet-laden, harmonically forced planar jets are conducted in an effort to better understand the underlying physics involved in such flows. Full two-way mass, momentum and energy coupling between phases are considered. The effects of particle time constant, carrier gas temperature and "degrees of coupling" on various turbulent gas and particle/droplet properties are numerically measured. The results indicate that the downstream particle dispersion is nearly independent of particle injection for one-way coupling cases. The previous findings related to particle size and preferential concentration are confirmed, as smaller particles tend to follow the flow and therefore do not preferentially concentrate, while larger particles are largely unaffected by the carrier gas and also do not preferentially concentrate. However, the moderately sized particles tend to cluster together in regions of low-strain, causing relatively low "local particle dispersion".

For two-way coupling cases, our results indicate that the finite thermal inertia of the droplets significantly alters the density profile of the jet, causing a modification of the instabilities that govern jet growth rate even for non-evaporating droplets. Thus, cooler particles/droplets injected into a hot jet tend to stabilize the jet and decrease its growth rate. As the mass-loading ratio increases, the slope of the jet half-width increases as well mainly due to momentum coupling and particle drag. This relationship is somewhat linear for the range of mass-loading ratios considered in this study. The production rate of the turbulent kinetic energy is found to be of opposite sign on the positive transverse side of the jet, indicating a significant sink of turbulent kinetic energy due to the particles. The feedback between phases is evident in the particle axial velocity and particle number density profiles and the relative magnitude of the Reynolds stress is found to decrease with increased mass-loading.

An effort has been made to clearly separate the turbulence modification due to temperature effects, particle drag, heat transfer and evaporative effects (e.g., added mass). We have found that the evaporative effects mainly contribute to the increased stability of the jets, as the evaporation decreases the temperature and increases the density of the carrier gas. The Reynolds stress is damped by the addition of the evaporation; hence, the production of turbulent kinetic energy is also decreased.

This study is part of a larger ongoing effort to understand inhomogeneous particle-laden two-phase turbulent flows with and without particle (or droplet) evaporation and combustion and to develop more accurate and robust subgrid-scale turbulence closure models for these flows.

Acknowledgements

This work is sponsored by the US Office of Naval Research under grant N00014-01-1-0843. Dr. Gabriel Roy is the Program Manager for this grant. Additional support is provided by the National Science Foundation under grant CTS0092665.

References

[1] J. Hinze, Turbulence, McGraw-Hill, New York, 1975.
[2] S. Pope, Turbulent Flows, Cambridge University Press, New York, 2000.
[3] P. Bernard, J. Wallace, Turbulent Flow, John Wiley & Sons, Inc., Hoboken, NJ, 2002.
[4] F. Hsiao, J. Huang, On the evolution of instabilities in the near field of a plane jet, Phys. Fluids A 2 (1990) 400–412.
[5] S. Stanley, S. Sarkar, Simulations of spatially developing two-dimensional shear layers and jets, Theor. Comput. Fluid Dyn. 9 (1997) 121–147.
[6] C. Kennedy, J. Chen, Mean flow effects on the linear stability of compressible planar jets, Phys. Fluids 10 (1998) 615–626.
[7] P. Colucci, Linear stability analysis of density stratified parallel shear flows, in: Proceedings of the Thirty-Second Aerospace Sciences Meeting & Exhibit, AIAA-94-0011, 1994.
[8] C. Crowe, M. Sommerfeld, Y. Tsuji, Multiphase Flows with Droplets and Particles, CRC Press, Boca Raton, FL, 1997.
[9] L. Fan, C. Zhu, Principles of Gas–Solid Flows, Cambridge University Press, New York, NY, 1998.
[10] J. Eaton, J. Fessler, Preferential concentration of particles by turbulence, Int. J. Multiphase Flow 20 (supplement) (1994) 169–209.
[11] J. Bellan, Perspectives on large eddy simulations for sprays: issues and solutions, Atomization Spray. 10 (2000) 409–425.
[12] C. Crowe, J. Chung, T. Troutt, Particle mixing in free shear flows, Prog. Energy Combust. Sci. 14 (1988) 171–194.
[13] V. Armenio, V. Fiorotto, The importance of the forces acting on particles in turbulent flows, Phys. Fluids 13 (2001) 2437–2440.
[14] F. Jaberi, Temperature fluctuations in particle-laden homogeneous turbulent flows, Int. J. Heat Mass Transfer 41 (1998) 4081–4093.
[15] F. Mashayek, Droplet–turbulence interactions in low-Mach-number homogeneous shear two-phase flows, J. Fluid Mech. 367 (1998) 163–203.
[16] F. Mashayek, Direct numerical simulations of evaporating droplet dispersion in forced low Mach number turbulence, Int. J. Heat Mass Transfer 41 (1998) 2601–2617.
[17] F. Mashayek, Numerical investigation of reacting droplets in homogeneous shear turbulence, J. Fluid Mech. 405 (2000) 1–36.
[18] R. Miller, J. Bellan, Direct numerical simulation of a confined three dimensional gas mixing layer with one evaporating hydrocarbon-droplet-laden stream, J. Fluid Mech. 384 (1999) 293–338.
[19] R. Miller, J. Bellan, Direct numerical simulation and subgrid analysis of a transitional droplet laden mixing layer, Phys. Fluids 12 (2000) 650–671.
[20] R. Miller, Effects of nonreacting solid particle and liquid droplet loading on an exothermic reacting mixing layer, Phys. Fluids 13 (2001) 3303–3320.
[21] R. Miller, K. Harstad, J. Bellan, Evaluation of equilibrium and non equilibrium evaporation models for many-droplet gas–liquid flow simulations, Int. J. Multiphase Flow 24 (1998) 1025–1055.
[22] T. Poinsot, S. Lele, Boundary conditions for direct simulations of compressible viscous flow, J. Comput. Phys. 101 (1992) 104–129.
[23] D. Rudy, J. Strikewerda, A nonreflecting outflow boundary condition for subsonic Navier–Stokes calculations, J. Comput. Phys. 36 (1980) 55–70.
[24] A. Ferrante, S. Elghobashi, On the physical mechanisms of two-way coupling in particle-laden isotropic turbulence, Phys. Fluids 15 (2003) 315–329.